POLITECNICO DI TORINO
Repository ISTITUZIONALE

Wave-to-grid modelling of wave energy converter farms: Mechanical versus grid-injected energy-maximisation

Original
Wave-to-grid modelling of wave energy converter farms: Mechanical versus grid-injected energy-maximisation / De Clerck, V., Said, H.A., Pasta, E.. - (2026), pp. 1-6. (International Conference on Smart Energy Systems and Technologies (SEST) 02-04 September 2026 Ciudad Real (ESP)) [10.1109/sest67798.2026.11712463].

Availability:
This version is available at: 11583/3016407 since: 2026-10-09T08:31:45Z

Publisher:
IEEE

Published
DOI:10.1109/sest67798.2026.11712463

Terms of use:

This article is made available under terms and conditions as specified in the corresponding bibliographic description in the repository

Publisher copyright
IEEE postprint/Author's Accepted Manuscript

©2026 IEEE. Personal use of this material is permitted. Permission from IEEE must be obtained for all other uses, in any current or future media, including reprinting/republishing this material for advertising or promotional purposes, creating new collecting works, for resale or lists, or reuse of any copyrighted component of this work in other works.

(Article begins on next page)

26 November 2026

Wave-to-grid modelling of wave energy converter farms: Mechanical versus grid-injected energy-maximisation

1st Viola De Clerck
MOREnergy Lab, DIMEAS
Politecnico di Torino
Turin, Italy
viola.declerck@polito.it

2nd Hafiz Ahsan Said
Centre for Ocean Energy Research
Maynooth University
Maynooth, Ireland
hafiz.ahsansaid@mu.ie

3rd Edoardo Pasta
DEIB
Politecnico di Milano
Milan, Italy
edoardo.pasta@polimi.it

***Abstract*—Wave Energy Converters (WECs) are typically controlled using hydrodynamic strategies aimed at maximising absorbed mechanical power, while grid-side converters are designed independently to ensure compliant power injection. This decoupled approach may lead to suboptimal wave-to-grid (W2G) performance. This paper investigates whether control parameters that maximise absorbed mechanical energy also maximise the net electrical energy delivered to the grid. An integrated W2G modelling framework is developed, coupling a hydrodynamic model of interacting WEC arrays based on the Cummins' formulation with the complete electrical conversion chain, including generator, rectifier, DC-link, and grid-connected inverter. A first-order impedance matching (IM) controller is adopted, and its parameter space is explored under different sea states to construct mechanical and grid-energy performance maps. The results reveal a consistent mismatch between the corresponding optimal controller settings. Mechanically suboptimal configurations can yield significantly higher net electrical energy, as highly oscillatory power profiles associated with IM increase mechanical reactive power and reduce the energy delivered to the grid. These findings show that maximising mechanical energy alone is not sufficient to achieve optimal W2G performance and highlight the need for integrated control strategies that explicitly account for the complete electrical conversion chain.**

***Index Terms*—Wave energy converters; WEC array; Wave-to-grid modelling; Energy-maximising control**

I. Introduction

Wave energy converters (WECs) represent a promising technology for the exploitation of ocean wave resources, offering a predictable and largely untapped source of renewable energy [1]. The performance of WEC systems is strongly influenced by control strategies, which regulate the interaction between the device and incident waves. WEC control techniques are required to maximise energy absorption while ensuring stable operation [2]. Existing literature largely focuses on mechanical power maximisation at the device level. In particular, energy-maximising control formulations have been widely investigated, many of which are based on impedance matching (IM) principles [3], enabling the WEC to operate in resonance and optimise the absorbed mechanical power, P_{mech}. In conventional WEC control architectures, the system is structured into two layers: a hydrodynamic control layer, aimed at maximising P_{mech} through the power take off (PTO) force control [4], and an electrical conversion stage responsible for voltage regulation, grid synchronisation, and power injection [5]. To manage the fluctuating nature of wave energy, this stage is commonly complemented by hybrid energy storage systems (HESSs), which smooth the generated power before grid injection, improve power quality [6]. Although wave-to-grid (W2G) frameworks model the full conversion chain [7], [8], optimisation is still commonly performed in a decoupled manner. Optimal WEC operation typically requires the PTO to exchange both active and reactive power [9]. It is important to note that the reactive power in WEC hydrodynamic control is different from the reactive power in electrical networks. In hydrodynamic WEC control, in fact, the reactive power corresponds to the negative (active) electrical power, rather than the electrical reactive power exchanged at the generator terminals.[1] From now on, the reactive power in hydrodynamic sense is referred to as 'mechanical reactive power', while the reactive power in electrical sense is referred to as 'electrical reactive power'.

While mechanical reactive power enables resonance and maximisation of P_{mech}, it does not directly contribute to net grid energy. Moreover, large reactive power peaks are often associated with practical limitations rather than intrinsic optimality [9]. Recent studies have therefore proposed strategies targeting usable electrical energy, including loss-aware approaches that account for conversion inefficiencies [1], [10]. These results indicate that maximising P_{mech} alone may not ensure optimal system-level performance. However, beyond conversion losses, additional aspects remain only partially explored. In particular, the impact of hydrodynamic control tuning on the full wave-to-grid energy conversion process has not been systematically analysed. In this context, a whole-system-oriented perspective is adopted to analyse the classical IM-based WEC optimisation problem. This study investigates the influence of control parameter tuning on both P_{mech} and P_{grid} by constructing performance maps over combinations of

[1]For more details on these differences, readers are referred to [6]

control parameters. This enables a direct comparison between configurations that maximise mechanical energy capture and those that yield higher usable electrical output. By analysing the trade-off between hydrodynamic energy absorption and effective electrical power delivery, the proposed approach identifies control configurations that, while suboptimal in terms of P_{mech}, improve net grid power injection. This highlights mismatches between classical hydrodynamic optimisation objectives and system-level performance, supporting the development of more integrated control strategies.

To this end, this work develops an integrated W2G modelling framework to investigate the relationship between hydrodynamic controller tuning and the resulting grid-level energy performance. This paper is organised as follows. Section II describes the proposed methodology and modelling framework. Section III presents the sensitivity analysis of the control parameter tuning. Section IV presents and discusses the main results and Section V provides the conclusions.

II. Methodology

The proposed system, shown in Figure 1, represents the complete W2G conversion chain of a single WEC device within a unified simulation environment. The power outputs of the individual devices are collected at the point of common coupling (PCC) prior to grid injection. Accordingly, each WEC is equipped with its own power conversion and conditioning chain, including a dedicated HESS, whose internal components are detailed in Section II-D4, and the associated control architecture. The case study considers an array composed of three identical WECs arranged in a triangular layout. Each WEC is modelled as a single-degree-of-freedom (DoF) spherical point absorber operating in heave, with a radius $r = 4.5\,\mathrm{m}$. The devices are positioned at an equal distance of $6r$ from the array centre, as illustrated in Figure 2.

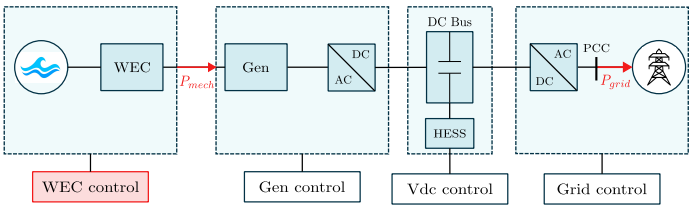

Fig. 1. Integrated W2G modelling and control framework for the WEC array.

A. WEC modelling

The WEC system is modelled using the linear potential-flow theory and the Cummins' equation formulation [11]. For an array of N interacting WECs, the vector of heave displacements is $\mathbf{z}(t)$. Under the assumptions of inviscid, incompressible, and irrotational flow, and small body motions, the array dynamics can be expressed in compact form as [12]

$$\left(\mathbf{M}+\mathbf{A}_{\infty}\right)\ddot{\mathbf{z}}(t)+\int_0^t \mathbf{K}_r(\tau)\,\dot{\mathbf{z}}(t-\tau)\,\mathrm{d}\tau+\mathbf{S}_h\,\mathbf{z}(t) = \mathbf{f}_{ex}(t)+\mathbf{f}_{pto}(t), \tag{1}$$

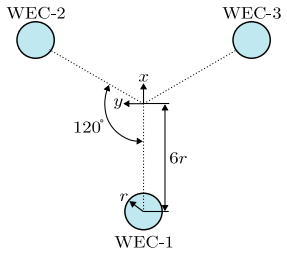

Fig. 2. WEC array composed of three point absorbers considered in the study.

where $\mathbf{M}, \mathbf{A}_{\infty}, \mathbf{K}_r, \mathbf{S}_h \in \mathbb{R}^{N\times N}$ represent the inertia, infinite-frequency added-mass, radiation impulse response, and hydrostatic restoring matrices, respectively, and $\mathbf{f}_{ex}(t), \mathbf{f}_{pto}(t) \in \mathbb{R}^N$ are the wave-excitation and PTO control force vectors. Frequency-domain hydrodynamic coefficients (added mass, radiation damping, excitation forces, and hydrostatic terms) are computed using a BEM solver with multi-body interaction. In this study, OrcaWave [13] is used.

B. Impedance matching control

The WEC array is controlled according to a standard IM strategy, introduced in Section I, with the objective of maximising the absorbed mechanical power P_{mech}. Within the farm, each WEC is equipped with an independent PTO controller acting on the corresponding device motion. For the i-th WEC, the PTO force is generated through a first-order (FO) dynamic controller acting on the device velocity, and is expressed in the Laplace domain as

$$f_{pto,i}(s) = \frac{\alpha s}{s+\beta}\,V_i(s), \tag{2}$$

where $V_i(s)$ is the Laplace transform of the device velocity $v(t) = \dot{z}_i(t)$, while α and β are the parameters defining the FO controller dynamics. For the sake of simplicity, the parameters α and β are assumed identical across all PTO controllers within the array, resulting in a decentralised control strategy. Although this approach may lead to reduced performance compared to centralised control, it is adopted for its lower implementation complexity [14]. This control structure represents a classical IM formulation, whereby the PTO imposes a target mechanical impedance tuned to the dominant wave characteristics, to match the optimal impedance condition [15]. Conventionally, a unique controller configuration is identified by selecting the parameter set that maximises the absorbed mechanical power based on linear hydrodynamic model. In this work, beyond the conventional IM formulation based on this linear model, a wide range of FO controller parameter set is explored through exhaustive simulations of the complete nonlinear W2G model, and the optimal parameter set is identified based on the corresponding simulation results. For each parameter combination, both mechanical and grid-level performance metrics are evaluated to enable a comparative analysis across the control parameter domain.

C. HESS design

The HESS is a key component of the W2G power conditioning chain, enabling smoothing of the grid-injected power [16], as detailed in Section II-D4. It consists of a battery and a supercapacitor, a widely adopted combination for offshore applications due to its favourable balance between energy capacity, power capability, and dynamic response [17]. Both devices are interfaced with the DC bus through bidirectional DC/DC converters and are sized according to the operating conditions considered, following the iterative sizing framework proposed in the authors' previous work [18], which identifies the minimum storage capacity satisfying the selected operating constraints. The state of charge (SOC) of both devices is defined as follows.

$$\dot{SOC}_{bat} = \frac{P_{bat}}{3600 V_{bat} C_{bat}} \tag{3}$$

$$\dot{SOC}_{sc} = \frac{P_{sc}}{\frac{1}{2} C_{sc} V_{sc}^2} \tag{4}$$

D. Power-to-grid chain modelling and control

The electrical conversion chain describes the dynamic energy transfer from the generator terminals to the grid interface. The overall modelling approach follows the wave-to-grid formulation presented in [7], whereas the electrical control architecture follows [19], [20], where the adopted control-oriented models and modelling assumptions are detailed. The system includes a linear permanent magnet generator (LPMG) with an active rectifier, a DC bus equipped with a HESS, and a grid-connected inverter.

1) Generator-side model and control: The LPMG dynamics are expressed in the rotating dq reference frame. Assuming equal d- and q-axis inductances ($L_d = L_q = L_s$), the stator current dynamics are given by:

$$\dot{i}_{ds} = -\frac{R_s}{L_s} i_{ds} + \omega_e i_{qs} - \frac{1}{L_s} v_{ds}, \tag{5}$$

$$\dot{i}_{qs} = -\omega_e i_{ds} - \frac{R_s}{L_s} i_{qs} - \frac{\omega_e}{L_s} \Psi_{pm} - \frac{1}{L_s} v_{qs}, \tag{6}$$

where i_{ds}, i_{qs} and v_{ds}, v_{qs} denote stator currents and voltages, R_s and L_s the stator resistance and inductance, Ψ_{pm} the permanent magnet flux linkage, and ω_e the electrical angular speed, proportional to the translator velocity (*i.e.*, $\omega = \frac{\pi}{\tau}\dot{z}$).

The generator-side control is implemented using proportional-integral (PI) current regulators, following the approach in [19]. The d-axis current reference is set to zero in order to minimize copper losses. While, following [7], [19], the q-axis current reference is derived as

$$i_{qs}^{ref} = -\frac{2\tau}{3\Psi_{pm}} f_{pto}^{ref}, \tag{7}$$

where τ is the pole pitch of the linear generator and f_{pto}^{ref} is the reference PTO force, defined in (2).

2) HESS model and control: The storage subsystem modelling follows [7]. The battery and supercapacitor currents dynamics are described by:

$$\dot{i}_{bat} = \frac{1}{L_{bat}} \left(V_{bat} - R_{bat} i_{bat} - v_{bat,t} \right), \tag{8}$$

$$\dot{i}_{sc} = \frac{1}{L_{sc}} \left(V_{sc} - R_{sc} i_{sc} - v_{sc,t} \right), \tag{9}$$

where i_{bat} and i_{sc} denote the battery and supercapacitor currents, V_{bat} and V_{sc} their nominal voltages, R and L the equivalent resistances and inductances and $v_{bat,t}$ and $v_{sc,t}$ respectively represents the terminal voltages.

HESS controller is computed according to the PI-based control strategy presented in [20]. The reference signals i_{bat}^{ref} and i_{sc}^{ref} are provided by the energy management system (EMS), described in Section II-D4. In addition to the EMS contribution, the HESS faces an additional component associated with DC bus voltage regulation, implemented through a PI controller as described in [20].

3) Grid-side inverter model and control: The grid-side converter is modelled in the synchronous dq frame aligned with the grid voltage. The currents dynamics are given by:

$$\dot{i}_{dg} = -\frac{R_f}{L_f} i_{dg} + \omega_g i_{qg} - \frac{1}{L_f} v_{dg} + \frac{1}{L_f} v_{dc} u_{dg}, \tag{10}$$

$$\dot{i}_{qg} = -\omega_g i_{dg} - \frac{R_f}{L_f} i_{qg} - \frac{1}{L_f} v_{qg} + \frac{1}{L_f} v_{dc} u_{qg}, \tag{11}$$

where i_{dg} and i_{qg} are the grid currents, v_{dg} and v_{qg} the grid voltages, R_f and L_f the filter parameters, ω_g the grid angular frequency, and u_{dg}, u_{qg} the inverter modulation signals. Following [7], the synchronous reference frame is aligned with the grid voltage through a phase-locked loop (PLL), such that v_{dg} and v_{qg} represent the grid voltage components expressed in the PLL-based dq frame.

The inverter operates according to [20]. Decoupled PI current controllers are employed, with electrical reactive current reference set to zero, to ensure unity power factor operation. The active current reference i_{dg}^{ref} is generated by the EMS based on the filtered WEC power and system constraints.

4) Energy management system: The EMS distributes the WEC electrical power among the grid, the battery, and the supercapacitor in order to generate the corresponding current references for the control stages. The EMS, whose scheme is presented in Figure 3, is composed of two cascaded low-pass filters (LPFs). The first performs grid power smoothing by extracting the low-frequency component of P_{wec} to be injected into the grid. The remaining power component is processed through a second LPF to allocate the low-frequency contribution to the battery, while the high-frequency component is assigned to the supercapacitor. This structure enables effective power smoothing for grid injection and coordinated energy sharing within the HESS.

5) DC bus dynamics and control: Finally, the DC bus voltage dynamics are governed by the current balance between generator-side, storage, and grid-side subsystems:

$$C_{dc} \dot{v}_{dc} = i_{gen} + i_{bat} + i_{sc} - i_{inv}, \tag{12}$$

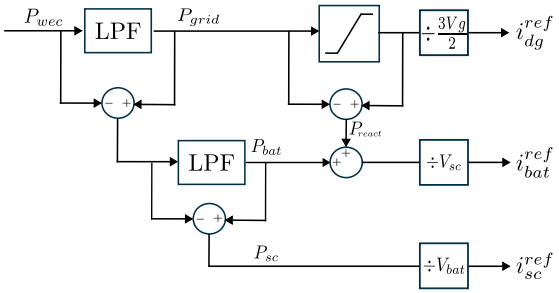

Fig. 3. Energy management system framework.

where C_{dc} is the DC bus capacitance, i_{gen} is the rectifier output current, and i_{inv} is the inverter input current.

As previously anticipated in Section II-D2, the DC voltage control is computed by the storage component.

III. Sensitivity Analysis

A sensitivity analysis is performed over the IM controller parameters (α, β) to evaluate their impact on both absorbed mechanical energy and grid-injected energy. As a reference condition, the controller parameters are first determined according to the classical IM approach, based on resonance conditions of the device for each sea state, and in particular on the wave energy period. This configuration provides the baseline tuning for mechanical energy maximisation. The analysis is then extended by defining a two-dimensional parameter space over selected ranges of α and β, discretised into a uniform heatmap. For each parameter pair, time-domain simulations are carried out under the considered sea states, and the corresponding absorbed mechanical energy and grid-injected energy are evaluated over a fixed simulation horizon. For each sea state, the collected results are used to construct performance maps over the (α, β) domain for both energy metrics. Once the maps are obtained, the parameter combinations corresponding to the maximum mechanical and grid energy are identified, leading to the definition of mechanical optimal (Mech Opt) and grid optimal (Grid Opt) parameters configurations, together with the baseline IM-based tuning.

IV. Results

The proposed W2G modelling framework is employed to assess the influence of the device controller on the electrical conversion chain and the resulting grid energy output. This analysis is conducted through numerical simulations of the considered WEC array under three representative sea states (SS1, SS2, SS3), characterised by the significant wave height (H_s) and the energy period (T_e), as summarised in Table I.

TABLE I
Parameters of sea states: SS1, SS2, SS3.

Sea State ID	H_s [m]	T_e [s]
SS1	2	4.5
SS2	2.5	6
SS3	3	8

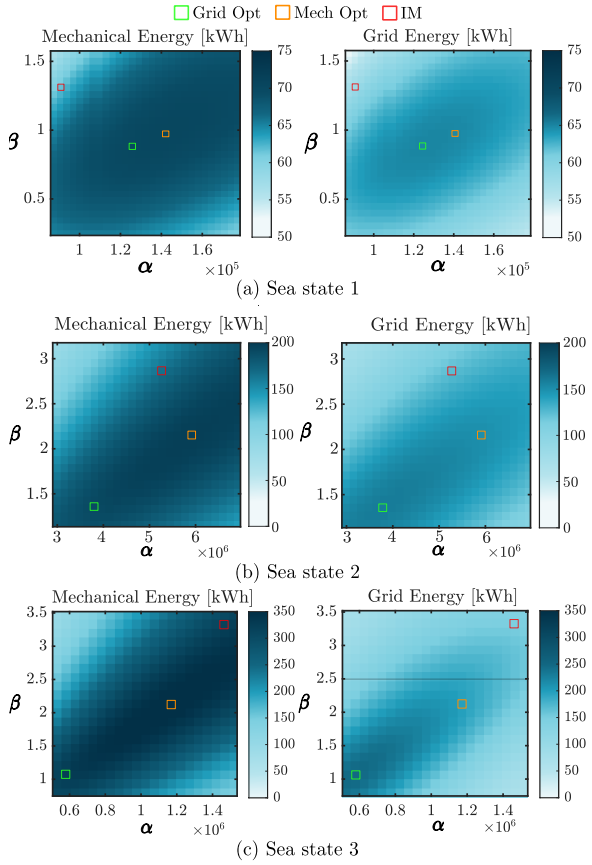

Fig. 4. Heatmap comparison of E_{mech} and E_{grid} versus α and β for the three sea states (SS1, SS2, SS3), with highlighted the three optimal combinations: IM, Mech Opt, Grid Opt.

The sensitivity analysis over the controller parameters (α, β) is employed to derive two-dimensional performance maps of the absorbed mechanical energy E_{mech} and the grid-injected energy E_{grid}, shown in Figure 4. The heatmap results reveal a consistent mismatch between the controller configurations that maximise E_{mech} and those that maximise E_{grid}. This discrepancy is observed across all sea states and becomes more pronounced for more energetic wave conditions (*i.e.*, SS3). In addition, the parameter region associated with classical IM tuning does not coincide with the actual mechanical optimum (Mech Opt). This deviation arises from the assumptions underlying IM-based design, typically formulated under linear hydrodynamic conditions and regular wave excitation, whereas the present analysis considers irregular sea states. In addition, the IM formulation neglects grid dynamics and their impact on the final energy output. Furthermore, the control parameters are optimised at the array level but implemented in a decentralised manner with identical parameters for all devices. As a result, the IM-based parameter selection does not necessarily yield the true mechanical optimum under realistic operating conditions. Additionally, Table II provides a quantitative comparison between the optimal configurations. For all sea states, the grid-optimal configuration (Grid Opt) yields higher E_{grid}, despite extracting less mechanical energy.

TABLE II
ENERGY AND EFFICIENCY COMPARISON FOR DIFFERENT CONTROL STRATEGIES AND SEA STATES.

Sea State	Opt	E_{mech} [kWh]	E_{grid} [kWh]	η [%]
SS1	Grid	70.13	**65.12**	92.9
	Mech	**70.37**	64.93	92.3
	IM	61.81	58.17	94.1
SS2	Grid	191.32	**160.05**	83.7
	Mech	**198.84**	150.01	75.4
	IM	165.73	124.38	75.0
SS3	Grid	324.38	**250.12**	77.1
	Mech	**353.96**	197.63	55.8
	IM	315.97	144.71	45.8

This behaviour is consistent across all sea states and becomes more pronounced under more energetic conditions, indicating a growing influence of the interaction between hydrodynamic control and the electrical conversion chain as the available wave energy increases. The IM-based configuration remains suboptimal in terms of both E_{mech} and E_{grid} across all sea states, consistently yielding lower energy levels than both the mechanical- and grid-optimal configurations (Table II). The overall conversion efficiency, computed as $\eta = E_{grid}/E_{mech}$, follows a similar trend, with comparable or slightly higher values under low-energy conditions (94.1% in SS1) and a marked reduction for more energetic states (45.8% in SS3). The higher efficiency of the IM approach observed in SS1 is primarily associated with reduced energy levels rather than improved conversion performance. Moreover, SS1 is closer to the resonance period of the device; therefore, the consistently high performance and limited variability among control strategies in this sea state are mainly attributable to resonance effects. For SS3, the Grid-Opt configuration increases the injected energy by approximately $+21\%$ compared to the mechanical optimum (from 198 kWh to 250 kWh), while reducing the absorbed mechanical energy by about 9% (from 354 kWh to 324 kWh). This results in a substantial improvement in overall conversion efficiency, from 55.8% to 77.1%. These results confirm that maximising E_{mech} does not necessarily lead to optimal grid-level performance and may instead result in suboptimal energy utilisation.

Further insight into the observed differences is provided by the time-domain power profiles in Figure 5. The Mech Opt and IM configurations exhibit highly oscillatory mechanical power, with pronounced peaks and significant bidirectional exchange, reflecting the presence of mechanical reactive power required for resonance and energy maximisation. However, a substantial portion of this oscillatory power does not contribute to net grid energy. Consequently, although E_{mech} is maximised, part of the absorbed energy is not effectively converted into grid-injected power, as confirmed by the smoother and lower-amplitude grid power profiles, where excess fluctuations and mechanical reactive power are absorbed by the HESS. The HESS behaviour is further analysed through the SOC profiles shown in Figure 6. The SOC profiles of both HESS

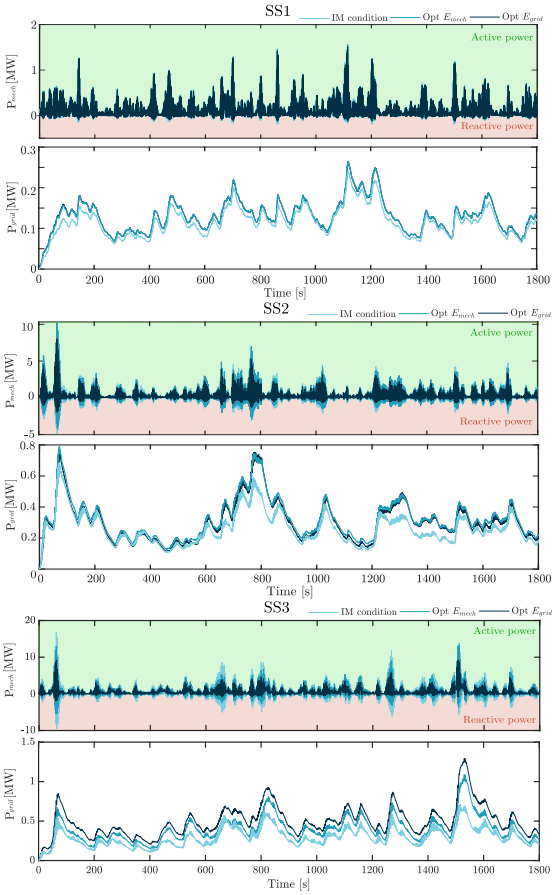

Fig. 5. Mechanical power P_{mech} and grid power P_{grid} profiles for the three controller configurations considered across the sea states (SS1, SS2, SS3): IM tuning, maximum mechanical energy, and maximum grid energy.

elements show consistently lower levels for the IM and Mech Opt configurations compared to the Grid Opt case. This behaviour is not directly associated with increased stress on the storage devices, but rather with the contribution required to compensate the mechanical reactive power demanded by the PTO. In particular, the battery also compensates for residual negative power components at the grid side after the filtering stage. From a storage dynamics perspective, the supercapacitor exhibits a more intermittent and highly fluctuating behaviour, as it is responsible for absorbing the fast power variations. In contrast, the battery presents a smoother SOC profile, associated with lower-frequency power components.

To sum up, the grid-optimal configuration, while still requiring mechanical reactive power, exhibits reduced oscillations and smoother power profiles, resulting in a higher fraction of usable energy delivered to the grid. These results indicate that, although mechanical reactive power is necessary for optimal energy absorption, the overall characteristics of the power profile, including its magnitude and temporal variability, strongly affect system-level performance. This explains the shift in the optimal parameter region in Figure 4, highlighting that highly oscillatory power profiles, while beneficial for maximising E_{mech}, can reduce overall conversion effectiveness.

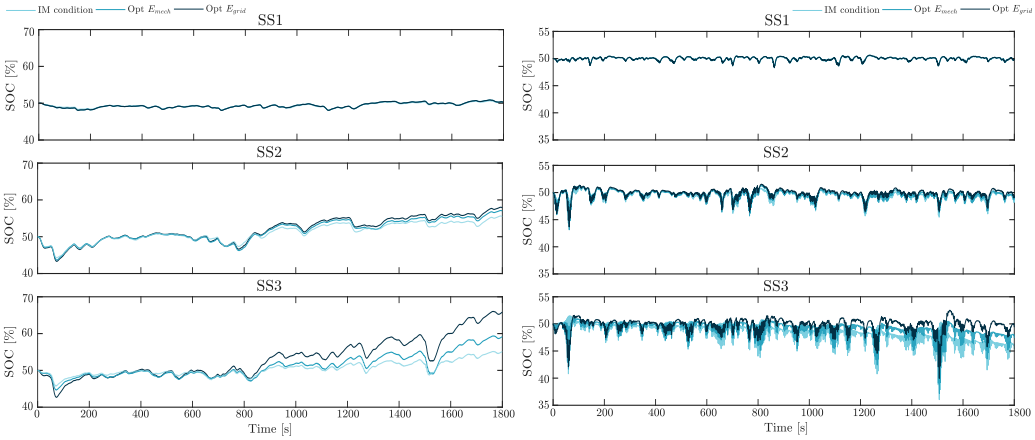

(a) Battery SOC (b) Supercapacitor SOC

Fig. 6. Battery (a) and supercapacitor (b) state of charge for the three different sea states (SS1, SS2, SS3) in the three optimal conditions (Grid Opt, Mech Opt, IM).

V. Conclusions

This paper investigated the relationship between hydrodynamic control tuning and grid-level performance in WEC arrays within a wave-to-grid (W2G) framework. The results reveal a clear mismatch between control configurations that maximise absorbed mechanical energy and those that maximise grid-injected energy. In particular, grid-optimal configurations achieve higher usable energy despite lower mechanical absorption, with this effect becoming more pronounced under energetic sea states. This behaviour is primarily linked to the characteristics of the power profiles. Highly oscillatory mechanical power, associated with classical IM-based and mechanically optimal tuning (Mech Opt), increases mechanical reactive power exchange and reduces the fraction of energy effectively delivered to the grid, whereas smoother profiles enable more efficient conversion. These findings demonstrate that maximising mechanical energy alone does not necessarily guarantee optimal system-level performance. Instead, achieving higher efficiency of the overall W2G conversion chain requires controller tuning that explicitly accounts for the full system dynamics. Future developments may include advanced control strategies (e.g., model predictive control), centralised control schemes, and loss-aware modelling within the W2G framework to further enhance system-level optimisation.

References

[1] X. Huang, Z. Lin, K. Chen, J. Zhou, and X. Xiao, "Improving wave-to-wire efficiency of direct-drive wave energy converters with loss-aware model predictive control and variable dc voltage control," *IEEE Trans. Ind. Electronics*, vol. 72, 2025.

[2] E. Pasta, N. Faedo, G. Mattiazzo, and J. V. Ringwood, "Towards data-driven and data-based control of wave energy systems: Classification, overview, and critical assessment," *Renewable Sustain. Energy Reviews*, vol. 188, 2023.

[3] N. Faedo, F. Carapellese, E. Pasta, and G. Mattiazzo, "On the principle of impedance-matching for underactuated wave energy harvesting systems," *Appl. Ocean Res.*, vol. 118, 2022.

[4] S. Sheshaprasad, F. Naghavi, S. Hasanpour, M. Albader, M. C. Gardner, H. Kang, and H. A. Toliyat, "Optimal electric power take-off strategy for surface riding wave energy converter," in *2022 IEEE Energy Convers. Congr. Expo. (ECCE)*, IEEE, 2022.

[5] G. Fan, W. Wu, H. Zhang, L. Cui, and F. Blaabjerg, "Evaluation of power generation capacity of wave energy converter with a controllable-valve buoy based on wave-to-grid modeling and control," *Ocean Eng.*, vol. 310, 2024.

[6] H. A. Said, "Grid integration aspects of wave energy," 2024.

[7] H. A. Said, D. García-Violini, and J. V. Ringwood, "Wave-to-grid (w2g) control of a wave energy converter," *Energy Convers. Management: X*, vol. 14, 2022.

[8] F. Dong, S. Pan, J. Gong, and Y. Cai, "Comprehensive wave-to-wire model and control strategy design for wave energy conversion system," *Ocean Eng.*, vol. 284, 2023.

[9] H. A. Said, D. Garcia-Violini, N. Faedo, and J. V. Ringwood, "On the ratio of reactive to active power in wave energy converter control," *IEEE Open J. Control Syst.*, vol. 3, 2024.

[10] Z. Lin, J. Zhou, X. Huang, K. Chen, X. Xiao, and J. V. Ringwood, "On loss-aware optimal control of wave energy converters with electrical power take-offs," *IEEE Trans. Sustain. Energy*, vol. 15, 2024.

[11] W. Cummins, "The impulse response function and ship motions. Technical Report 1661," tech. rep., Dept. of the Navy, David Taylor model basin, Washington DC, 1962.

[12] E. Pasta, G. Papini, Y. Peña-Sanchez, F. D. Mosquera, F. Ferri, and N. Faedo, "Data-based modelling of arrays of wave energy systems: Experimental tests, models, and validation," *Control Eng. Pract.*, vol. 148, 2024.

[13] Orcina Ltd., "OrcaWave Documentation," 2023.

[14] Z. Lin, X. Huang, Y. Han, X. Xiao, and J. V. Ringwood, "Fast centralized model predictive control for wave energy converter arrays based on rollout," *IEEE Trans. Sustain. Energy*, vol. 16, 2025.

[15] B. Paduano, F. Carapellese, E. Pasta, S. A. Sirigu, N. Faedo, and G. Mattiazzo, "Data-based control synthesis and performance assessment for moored wave energy conversion systems: The pewec case," *IEEE Trans. Sustain. Energy*, vol. 15, no. 1, 2024.

[16] S. Rasool, K. M. Muttaqi, and D. Sutanto, "A multi-filter based dynamic power sharing control for a hybrid energy storage system integrated to a wave energy converter for output power smoothing," *IEEE Trans. Sustain. Energy*, vol. 13, no. 3, 2022.

[17] X. Lin and R. Zamora, "Controls of hybrid energy storage systems in microgrids: Critical review, case study and future trends," *J. Energy Storage*, vol. 47, 2022.

[18] V. De Clerck, H. A. Said, B. Paduano, E. Pasta, *et al.*, "A comparative study on basic design of hybrid storage architectures for grid-connected arrays of wave energy converters," in *Proc. Eur. Wave Tidal Energy Conf.*, vol. 16, 2025.

[19] M. I. Ullah, I. Temiz, J. Forslund, and J. S. Döhler, "Power quality assessment of a wave energy converter using energy storage," in *Proc. Eur. Wave Tidal Energy Conf.*, vol. 15, 2023.

[20] M. I. Ullah, *Advanced Converter Control Strategies for Wave Energy Systems: Energy Storage System, Power Quality Assessment and Remote Island Electrification*. PhD thesis, Acta Universitatis Upsaliensis, 2025.